J Fail. Anal. and Preven.
DOI 10.1007/s11668-016-0157-3

TECHNICAL ARTICLE—PEER-REVIEWED

Corrosion of Aluminum Alloy Metal Matrix Composites in Neutral Chloride Solutions

Roland Tolulope Loto · Adeyinka Adeleke

Submitted: 4 May 2016 / in revised form: 14 July 2016

Abstract The electrochemical behavior of UNS A0332.00S, UNS A0332.20S, UNS A0359.00S, and UNS A0359.20S aluminum alloys were studied in NaCl media through weight loss, potentiodynamic, and cyclic polarization techniques. UNS A0332.20S and UNS A0359.20S were reinforced with SiC, 20% by volume while the other two samples were not reinforced. Scanning electron microscopy and energy dispersive spectroscopy were used to analyze the role of intermetallic phases in both the corroded and non-corroded aluminum alloy samples. Results showed that unreinforced alloys have lower corrosion rates compared to the reinforced alloys. Pits on the reinforced alloys were significantly more numerous, shallower, and widespread than on the monolithic alloys. Al/SiC interface particles and intermetallic phases were observed to form at the mouth of the pits especially in alloys reinforced with SiC particles which might have contributed significantly to the weakening of regions where localized corrosion occurs. The result shows that intermetallic phases may directly influence the corrosion behavior of the aluminum alloys.

R. T. Loto (✉)
Department of Mechanical Engineering, Covenant University, Ota, Ogun State, Nigeria
e-mail: tolu.loto@gmail.com

A. Adeleke
Corrosion & Materials Engineer, Houston, TX, USA

A. Adeleke
Department of Mechanical Engineering, King Fahd University of Petroleum & Minerals, Dhahran 31261, Kingdom of Saudi Arabia

Keywords Corrosion · Aluminum · Composite materials · Pitting

Introduction

Metal matrix composites are the focus of attention of automobile, electronics, aerospace, and military industrial complex due to their high-temperature applications, strength-to-weight ratio, stiffness, and dimension stability on thermal recycling. There has been lots of enthusiasm concerning the application of metal matrix composites in corrosive environments. Aluminum alloys such as 2024, 5052, 6061, and 7071 have been largely employed as matrix materials with silicon carbide (particles) as their major alloying element. Al/SiC composites undergo more rapid deterioration due to localized corrosion than their homogeneous counterparts [1, 2]. The localized corrosion which occurs at preferential sites can be attributed to factors, such as the unstable silicon carbide matrix, existence of crevices, cracks, and pores, processing routes, existence of secondary phases, and the percentage volume of reinforcement of SiC. A number of small volume intermetallic precipitates forms on the composite in comparison to the alloy. This suggests the probability of the formation of a significant number of secondary phases being accelerated by silicon carbide. A higher volume fraction of the composite has been observed to increase the likelihood of localized corrosion reactions. Past research on alloy 6013-20 SiC, shows the presence of localized corrosion on secondary phases [2].

The duplex nature of the composites aggravates corrosion on the alloy surface and within the matrix compared to their homogeneous alloys [3–6]. This limits the service

Published online: 30 August 2016

lifespan and cause accelerated degradation of their exceptional mechanical properties, the main purpose for which it is designed. Currently there is strong interest in the corrosion behavior and electrochemical properties of complex aluminum alloys prepared by special techniques, such as rapid solidification processing, laser surface melting, and surface modification of the ion beam technique [7–11]. B/Al composite experienced 50% deterioration in the transverse strength after immersion in 3.5 wt.% NaCl for six hours [12]. Al 6061/SiC shows a higher magnitude of pitting corrosion compared to the corresponding unreinforced aluminum alloy [13, 14]. The pits were observed to be shallower, but more numerous than the unreinforced alloy [15]. The silicon carbide/Al interface is presumed to be the preferred site for pit initiation and propagation [16]. Extruded composites were observed to have mild corrosion damage due to the absence of flaws such as gas pores and greater homogeneous distribution of the particles [17] compared to the unreinforced alloys. Research has shown that the presence of SiC alters the growth of corrosion pits [18]. The market potential of Al6061/SiC makes it the most widely used test material for corrosion investigation in recent years.

SiC has been shown to be the preferred site for corrosion on Al 6061/SiC and Al 6013/SiC from previous work [19, 20]. The wrought alloy has a lower number of pits formed compared to the composite alloys. Composites tend to corrode faster than the main alloy matrix with the attack confined to the interface. Some researchers suggest that pitting corrosion initiates at SiC particles, while others suggest that SiC is not the preferred site for pit initiation. Research has shown that SiC causes microstructural changes in the alloy matrix, which influences the corrosion reaction mechanism [18–20]. The microstructure plays a major role in the electrochemical characteristics of Al/SiC composites. Pits in Al 5456/SiC have been shown to nucleate at microstructural secondary phases within the metal matrix [14]. Energy dispersive spectroscopy analysis of a pitted region in Al 5456 showed the presence of intermetallic precipitates consisting of major alloying elements including Mg, Cr, Al, Mn, and Fe as impurity. Observation shows that the composite (Al 5456/SiC) contained a significantly larger volume of smaller intermetallic precipitate than the wrought alloy [21].

The susceptibility of composites to localized corrosion is consistent with the inherent tendency of duplex systems to experience accelerated corrosion, thus controlling the number of suspected sites of localized corrosion that can possibly minimize corrosion of composites. The challenge for greater application of composites, in particular Al 6061/SiC, has increased with focus on service life and resistance to environmental degradation. This can be realized through understanding of the corrosion processes, the intriguing nature of silicon carbide particles, and their influence on the secondary phases and microstructure. This investigation aims to establish the role of secondary phases in relation to silicon carbide particles and microstructures in the localized corrosion processes as a step further to incorporate corrosion control in design and make these alloys more viable for technological applications.

Experimental Procedure

Material

Four samples of aluminum alloy samples were used for the experiment. Their percentage elemental compositions are shown in Table 1. Two of the alloy samples were reinforced with SiC particles, while the other two were not. The reinforced samples have contained about 98% SiC with particle size distribution of 12.8 μm ± 1.0 μm.

The mechanical properties of the aluminum samples before exposure are presented in Table 2. The manufacturing process conditions for each material are also indicated.

Test Environment

3.5 wt.% NaCl solution in the deaerated condition was used throughout the experiment. Deaeration was achieved by passing nitrogen gas, (N_2), through the solution until it became saturated with 99.5% N_2.

Table 1 Composition of the aluminum alloy samples

Alloy sample	% Composition											
	Si	Fe	Cu	Mn	Ni	Ti	Zn	Sr	Pb	Others	Al	SiC
UNS A0359.00S	9.5–10.5	0.8–1.0	3.0–3.5	0.5–0.8	1.0–1.5	0.20 max	0.03	0.005–0.015	…	0.10	Remain	0.0
UNS A0359.20S	9.5–10.5	0.8–1.0	3.0–3.5	0.5–0.8	1.0–1.5	0.20 max	0.03	0.005–0.015	…	0.10	Remain	19.0–22.0
UNS A0332.00S	9.5–10.5	0.2 max	2.8–3.2	0.8–1.2	1.0–1.5	0.20 max	0.05	0.000	…	0.10	Remain	0.0
UNS A0332.20S	9.5–10.5	0.2 max	2.8–3.2	0.8–1.2	1.0–1.5	0.20 max	0.05	0.000	…	0.10	Remain	18.0–22.0

Table 2 Mechanical properties of materials used (measured values)

Alloy identification	Ultimate tensile strength (Mpa)	Modulus of elasticity (Gpa)	Yield strength (MPa)	Elongation %	Temper
UNS A0359.00S	324	87	262	0.6	T6
UNS A0359.20S	359	98.6	332	0.4	T6
UNS A0332.00S	240	94	172	0.3	T5
UNS A0332.20S	283	101	269	0.2	T5

T5 Artificially aged only, *T6* solution heat treated and artificially aged

Sample Dimensions and Preparation

The sample dimensions for weight loss analysis were 20 mm × 20 mm for each specimen. The exposed area was 9.6 cm^2. Potentiodynamic and cyclic polarization analyses were performed on samples with circular dimension of 16 mm diameter. The exposed surface area was 1 cm^2, calculated with an accuracy ±1%. The same sample dimension was used for micro-analytical studies (scanning electron microscopy and energy dispersive spectroscopy). Grinding and polishing processes were performed on all the specimens to remove some minor scratches present on the surfaces. The samples for weight loss were washed in a hot detergent for five minutes and then rinsed with distilled water before exposure to solution containing potassium dichromate, 28 ml of phosphoric acid, and de-mineralized water to make 1 l of solution and then degreased. Cleaning was performed in an ultrasonic cleaner in distilled water. The samples were later dried in a desiccator for 24 h after cleaning. The dried samples were weighed with an analytical balance with an accuracy of ±0.5 mg. This procedure was followed after each test period for the corroded samples in accordance with ASTM standard G572 (85).

Circular disk specimens for the polarization experiments were ground with 320, 400, and 600 grit silicon carbide, in sequential order, to remove the coarse scratches. Polishing was carried out with 0.3 μm silicon carbide abrasive particles and final polishing was done with 0.05 μm abrasive particles. The specimens were then treated with boiling benzene and 5% acetic acid for five to ten minutes, rinsed in acetone, washed with de-mineralized water, air dried, and stored in a desiccator for 24 h prior to the commencement of the experiment.

Weight Loss Experiment

The effects of corrosion on the alloys were evaluated by weight loss method at 25 °C within an accuracy of ±3 °C. The amount of metal removed was determined by weighing the specimens before and after exposure. Weight loss was determined after every 200 h of exposure. The maximum period of exposure was 1600 h. As recommended by ASTM standard (G31-72), the experiments were performed under static conditions in a de-aerated solution. The corrosion rate is calculated from the weight loss and exposure time data. The corrosion rate (R) was calculated from Eq 1 below:

$$R = \left[\frac{87.6W}{DAT}\right] \quad \text{(Eq 1)}$$

W is the weight loss (g), D is the density (g/cm^2), A is the surface area in cm^2, and T is the exposure time (h).

Potentiodynamic and Cyclic Polarization

A potentiostat Model EG & G 273 A, interfaced with IBM PC 286 computer was used to evaluate the pitting resistance of the alloys being investigated. A polarization cell consisting of a reference, auxiliary, and working electrodes was connected to the potentiostat. All potentials were determined with respect to a saturated calomel electrode (SCE). A high-density graphite electrode was used as a counter electrode. The working electrode comprised the specimen holder, mounting rod, and the electrode holder. Both potentiodynamic and cyclic polarization analyses were carried out under the same experimental conditions. After maintaining a constant open circuit potential, the experiment began. Initial potential, for the potentiodynamic, was fixed at −0.25 mV (SCE) with scan rate of about 0.5 mV/s. Final potential was equally fixed at 0.8 mV (SCE). For cyclic polarization analysis, forward scan was fixed from −0.5 to 1.5 V (SCE) with scan rate of 5 mV/s and reverse scan was fixed from 1.5 to −0.8 V (SCE) with scan rate of 2.5 mV/s. The pitting potential (E_p), in each case, was determined by the extrapolation of polarization curve. In cyclic polarization, the protection potential (E_{pp}) was computed from the cyclic polarization scans when the reverse scan coincides with the forward scan closing the throughput loop. The corrosion current (i_{corr}), corrosion current density (I_{corr}), and corrosion potential (E_{corr}) were determined from the Tafel plots of potential versus log I_{corr}. The corrosion rate (R) was calculated from Eq 2;

$$R = \frac{0.00327 \times I_{corr} \times E_q}{D}, \quad \text{(Eq 2)}$$

where I_{corr} is the current density ($\mu A/cm^2$), D is the density (g/cm^3), E_q is the specimen equivalent weight (g).

Results and Discussion

Weight Loss Measurements

The comparative plots of corrosion rates versus exposure time in 3.5% NaCl solution for the aluminum alloys UNS A0359.20S, UNS A0359.00S, UNS A0332.20S, and UNS A0332.00S, are shown in Fig. 1. The results are summarized in Tables 3, 4, 5, and 6. Observation of the plots shows an initial increase in corrosion rate with respect to time. At specific time periods, the plots attain the maximum level followed by a sudden decrease in corrosion rate with respect to time. The latter section of the curves shows a substantial, but generally constant corrosion rate over a specified time period. The initial behavior of this process can be attributed to the gradual response of aluminum alloy constituents to Cl^- ions in the NaCl solution [22–27]. This occurs for alloys that passivate in aggressive environments. The formation of the oxide film on the alloy surface occurs gradually resulting in the initial increase in corrosion rate with respect to time. With the formation of the protective film, increase in corrosion rate ceases. At a certain stage the protective oxide film undergoes rupture, when the film breakage is faster than the rate of repassivation which leads to relatively constant corrosion rate with respect to time. This rupture phenomenon is assumed to have occurred due to residual tension created between the oxide film layer and aluminum matrix [28]. The corrosion on the aluminum alloy surface tends to be localized as a result of the redox

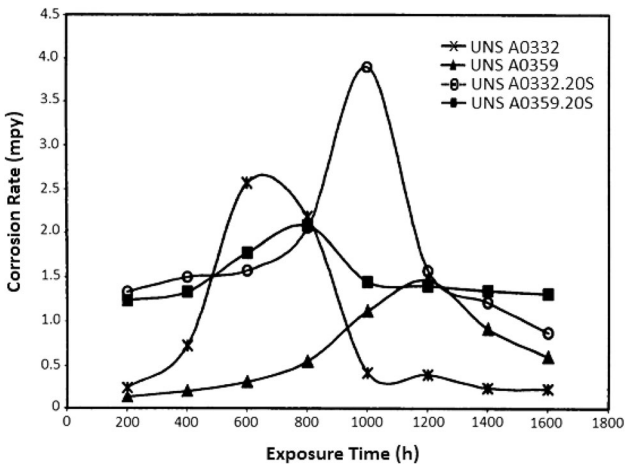

Fig. 1 Comparison of corrosion rate vs. exposure time graphs for the four alloys used

electrochemical solution resistance. The basic reaction at the anode is metal degradation:

$$Al \rightarrow Al^{3+} + 3e^- \quad \text{(Eq 3)}$$

While the cathodic reactions are oxygen reduction:

$$O_2 + 2H_2O + 4e^- \rightarrow 4OH \quad \text{(Eq 4)}$$

and or hydrogen reduction within a pit environment as a result of aluminum ion hydrolysis:

Table 3 Weight loss result for UNS A0359.20S

Sample	Weight loss (mg)	Weight loss average (mg)	Exposure time (h)	Corrosion rate	
				mpy	mm/year
1a	0.0023	0.0019	200	1.2312	0.0313
1b	0.0014		200		
2a	0.0036	0.0040	400	1.3310	0.0332
2b	0.0044		400		
3a	0.0073	0.0080	600	1.7747	0.0451
3b	0.0087		600		
4a	0.0118	0.0125	800	2.0797	0.0528
4b	0.0132		800		
5a	0.0080	0.0108	1000	1.4442	0.0367
5b	0.0137		1000		
6a	0.0138	0.0126	1200	1.3976	0.0355
6b	0.0114		1200		
7a	0.0143	0.0142	1400	1.3500	0.0343
7b	0.0141		1400		
8a	0.0104	0.0158	1600	1.3102	0.0333
8b	0.0211		1600		

Table 4 Weight loss result for UNS A0359.00S

Sample	Weight loss (mg)	Weight loss average (mg)	Exposure time (h)	Corrosion rate	
				mpy	mm/year
1a	0.0003	0.0002	200	0.1331	0.0034
1b	0.0001		200		
2a	0.0004	0.0006	400	0.1997	0.0052
2b	0.0008		400		
3a	0.0004	0.0014	600	0.3105	0.0078
3b	0.0024		600		
4a	0.0018	0.0033	800	0.5488	0.0139
4b	0.0048		800		
5a	0.0063	0.0084	1000	1.1180	0.0284
5b	0.0105		1000		
6a	0.0125	0.0132	1200	1.4639	0.0372
6b	0.0139		1200		
7a	0.0088	0.0097	1400	0.9220	0.0234
7b	0.0106		1400		
8a	0.0063	0.0072	1600	0.5990	0.0152
8b	0.0081		1600		

Table 5 Weight loss result for UNS A0332.20S

Sample	Weight loss (mg)	Weight loss average (mg)	Exposure time (h)	Corrosion rate	
				mpy	mm/year
1a	0.0042	0.0038	200	1.3289	0.0332
1b	0.0034		200		
2a	0.0010	0.0045	400	1.4974	0.0380
2b	0.0080		400		
3a	0.0052	0.0062	600	1.5752	0.0400
3b	0.0072		600		
4a	0.0191	0.0184	800	2.0599	0.0523
4b	0.0177		800		
5a	0.0456	0.0368	1000	3.8981	0.0990
5b	0.0280		1000		
6a	0.0324	0.0232	1200	1.5728	0.0399
6b	0.0140		1200		
7a	0.0162	0.0128	1400	1.2169	0.0309
7b	0.0094		1400		
8a	0.0122	0.0106	1600	0.8818	0.0224
8b	0.0090		1600		

Table 6 Weight loss result for UNS A0332.00S

Sample	Weight loss (mg)	Weight loss average (mg)	Exposure time (h)	Corrosion rate	
				mpy	mm/year
1a	0.0033	0.0019	200	0.2454	0.0062
1b	0.0005		200		
2a	0.0009	0.0052	400	0.7303	0.0185
2b	0.0095		400		
3a	0.0482	0.0296	600	2.5653	0.0651
3b	0.0110		600		
4a	0.0169	0.0312	800	2.1886	0.0556
4b	0.0456		800		
5a	0.0102	0.0092	1000	0.4224	0.0107
5b	0.0082		1000		
6a	0.0086	0.0064	1200	0.3985	0.0101
6b	0.0042		1200		
7a	0.0064	0.0050	1400	0.2456	0.0062
7b	0.0036		1400		
8a	0.0032	0.0041	1600	0.2325	0.0059
8b	0.0050		1600		

$$2H^+ + 2e^- \rightarrow H_2 \quad \text{(Eq 5)}$$

The association between miniature cathodes and anodes with the alloy matrix results in pitting corrosion, selective deterioration, intermetallic particle etchout, and corrosion at the grain boundaries. The oxide protective film that develops on the aluminum alloy surface is non-homogeneous, thin, and disordered. It provides an appreciable level of protection under appropriate conditions. When exposed to environments with chloride ions (Cl^-) (widely encountered), the oxide film breaks down at definite sites causing the formation of pits on the aluminum surface [29]. The solubility of Al^{3+} enables the degradation of the aluminum substrate metal and enhances accelerated chloride attack.

Observation of the results shows that UNS A0359.20S alloy has the highest corrosion rate of about 2.0797 mpy after 800 h of exposure. UNS A0359.00S alloy had a maximum corrosion rate of 1.4639 mpy after 1400 h. These results show that UNS A0359.00S alloy forms a protective layer of oxide earlier than its reinforced counterpart. The same trend of results was observed in UNS A0332.00S and UNS A0332.20S alloys. UNS A0332.20S alloy had its maximum corrosion rate of 3.898mpy after 1000hrs and UNS A0332.00S alloy had its maximum corrosion rate of 2.565 mpy after 600 h. With these results, UNS A0332.00S alloy forms protective film earlier enough before UNS A0332.20S alloy. The data above can be elucidated through consideration of the fact that aluminum and its alloys react in an unusual manner because they are amphoterics [30] and [31].

Comparison was made between unreinforced alloys, UNS A0359.00S and UNS A0332.00S, and the reinforced alloys, UNS A0359.20S and UNS A0332.20S alloys. The alloy with least corrosion rate is believed to be the alloy with highest corrosion resistance. UNS A0359.00S showed the lowest corrosion rate values, thus the alloy with highest corrosion resistance (Table 4). The corrosion rate values prove that it is the most suitable alloy for application in NaCl environment. Reinforced alloys (UNS A0359.20S and UNS A0332.20S) displayed the lowest corrosion resistance in comparison to the unreinforced UNS A0359 and UNS A0332 alloys (Fig. 1; Tables 3, 4, 5, and 6). These observations are in agreement with previous research, that alloys reinforced with SiC have lower corrosion resistance coupled with higher strength, than unreinforced alloys of the same matrix [32–35].

Potentiodynamic Polarization Test

Three different potentiodynamic polarization tests were performed for each of the aluminum alloys at ambient temperature to enable reproducibility of results under the same experimental conditions. Open circuit potential (OCP) was observed within the range of −0.500 and −0.557 V for UNS A0359.00S alloy. The range indicates the stability region of corrosion potential of the particular alloy. UNS A0359.00S alloy displayed open circuit potential values between −0.683 V and −0.765. The OCP values for UNS A0332.00S and UNS A0332.20S were also found to be in the range of −0.483 to −0.549 V and −0.497 to −0.564 V, respectively.

Table 7 Potentiodynamic polarization results for UNS A0359.20S from Tafel and polarization resistance calculations

Sample	Corrosion current, I_{corr} (μA)	OCP (V)	Ba (V/dec)	Bc (V/dec)	Corrosion rate (mpy)	
					Tafel cal.	Rp cal.
1C-1	0.6202	−0.683	0.0603	0.0994	0.347	1.700
1C-2	0.5314	−0.721	0.0689	0.1468	0.886	3.341
1C-3	0.9029	−0.763	0.0654	0.0974	1.688	2.688

Table 8 Potentiodynamic polarization results for UNS A0359.00S from Tafel and polarization resistance calculations

Sample	Corrosion current, I_{corr} (μA)	OCP (V)	Ba (V/dec)	Bc (V/dec)	Corrosion rate (mpy)	
					Tafel cal.	Rp cal.
1B-1	0.8476	−0.500	0.1236	0.2495	0.762	3.734
1B-2	0.6214	−0.553	0.1162	0.3839	0.234	1.123
1B-3	0.4299	−0.539	0.1107	0.3616	0.523	2.510

Table 9 Potentiodynamic polarization results for UNS A0332.20S from Tafel and polarization resistance calculations

Sample	Corrosion current, I_{corr} (μA)	OCP (V)	Ba (V/dec)	Bc (V/dec)	Corrosion rate (mpy)	
					Tafel cal.	Rp cal.
1B-1	0.4476	−0.524	0.1842	0.2578	1.489	3.742
1B-2	0.6722	−0.496	0.2000	0.1952	0.781	2.749
1B-3	0.9541	−0.560	0.2242	0.1950	1.286	3.503

Tafel and polarization resistance methods were used to determine the rate of corrosion for each of the aluminum alloys. In agreement with the results obtained from weight loss analysis, UNS A0359.00S alloy showed the lowest corrosion rate (0.762 mpy) compared to the other three aluminum alloys used from the Tafel approach (Table 7). This is sequentially followed by UNS A0332.00S with corrosion rate of 0.93 mpy. UNS A0332.20S and UNS A0359.20S have the highest corrosion rates with values of 1.489 and 1.688 mpy, respectively. A similar trend of result was observed with xxthe used of polarization resistance technique (Tables 7, 8, 9, and 10). Interpretation of the result shows that UNS A0359.00S alloy has the highest corrosion resistance capability while lowest resistance to corrosion was displayed in its reinforced counterpart, UNS A0359.20S alloy.

The corrosion rate results for UNS A0332.20S and UNS A0359.20S shows that the passive film in the SiC-reinforced alloys rapidly weakens and deteriorates at specific sites causing collapse of the protective film and pitting corrosion due to the presence of the intermetallic precipitates and its influence on the Cl^- interactions on the oxide film in NaCl solution [36–39]. The intermetallic or possibly the formation of secondary precipitates serve as susceptibility sites at the boundaries between grains for breakdown of the oxide film leading to localized corrosion reactions [40]. It is suggested that a competitive adsorption of chloride and hydroxide ions accelerates ion transport at the local defect sites lead to film thinning. Breakage of the protective oxide film leads to anion penetration and migration through the passive film [41–43].

Table 10 Potentiodynamic polarization results for UNS A0332.00S from Tafel and polarization resistance calculations

Sample	Corrosion current, $I_{corr.}$ (μA)	OCP (V)	Ba (V/dec)	Bc (V/dec)	Corrosion rate (mpy)	
					Tafel cal.	Rp cal.
1B-1	0.3804	−0.547	0.1176	0.1955	0.936	3.324
1B-2	0.6524	−0.537	0.2489	0.5462	0.541	2.597
1B-3	0.9735	−0.479	0.1128	0.2266	0.764	2.667

Chloride reactions result in the formation of soluble chlorinated aluminum hydroxide which hinders the stability of the oxide on the aluminum surface [44]. The presence of Si in conjunction with Mg allows Mg_2Si particles to precipitate [45–48]. Though it increases strength of the aluminum alloy, it makes the alloy susceptible to localized corrosion [49]. The recent investigation of the electrochemical behavior of Mg_2Si shows that Mg_2Si undergoes rapid dissolution compared to the matrix in Al alloys. Si seems to reside along the grain boundary which eventually leads to intergranular attack and stress corrosion cracking [50–52]. The presence of Cu within the aluminum alloy is deleterious to corrosion prevention as a result of the formation of cathodic sites responsible for prolonging the oxygen reduction reactions locally such as Al_2Cu and $AlCu_2Mg$. The precise role of Cu in the aluminum alloy matrix is still debatable. Muller and Galvele [53] reported an increase in pitting potential value for the elemental composition of Cu up to 5 wt.%. Cu-containing particles have also been observed to support sufficient oxygen reduction reactions [54–57].

Cyclic Polarization Techniques

The results obtained from the cyclic polarization test are summarized in Table 11 and the hysteresis loops obtained are shown in Figs. 2 and 3. Observation of the difference between the pitting potential (E_{pit}) and open

Table 11 Summary of the results obtained from cyclic polarization experiment

Sample	E_{pit} (V)	E_{pp} (V)	$E_{corr.}$ (V)	$E = E_{corr.} - E_p$ (V)	$E = E_{corr.} - E_{pit}$ (avg) (V)
UNS A0359.20S-1	−0.5890	−0.7170	−0.4760	0.1110	0.1386
UNS A0359.20S-2	−0.4110	−0.6220	−0.6210	0.2100	
UNS A0359.20S-3	−0.4240	−0.6820	−0.5120	0.0880	
UNS A0359.00S-1	−0.4880	−0.5120	−0.5930	0.1050	0.1550
UNS A0359.00S-2	−0.4110	−0.6220	−0.6200	0.2090	
UNS A0359.00S-3	−0.4100	−0.5020	−0.5620	0.1510	
UNS A0332.20S-1	−0.4120	−0.6120	−0.5030	0.0910	0.1236
UNS A0332.20S-2	−0.3960	−0.5570	−0.5250	0.1290	
UNS A0332.20S-3	−0.3650	−0.5620	−0.4760	0.1110	
UNS A0332.00S-1	−0.5360	−0.5640	−0.6360	0.1000	0.1527
UNS A0332.00S-2	−0.4130	−0.6040	−0.5940	0.1810	
UNS A0332.00S-3	−0.5210	−0.6030	−0.6980	0.1770	

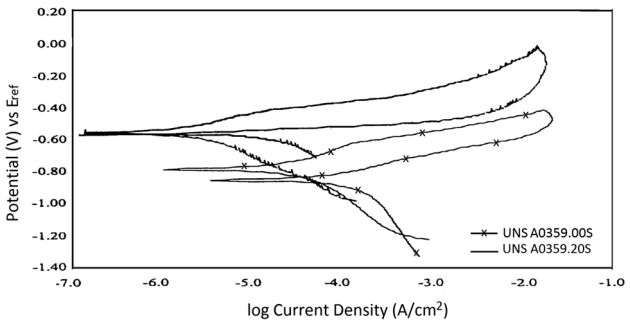

Fig. 2 Comparison of cyclic polarization curves for UNS A0359.00S and UNS A0359.20S

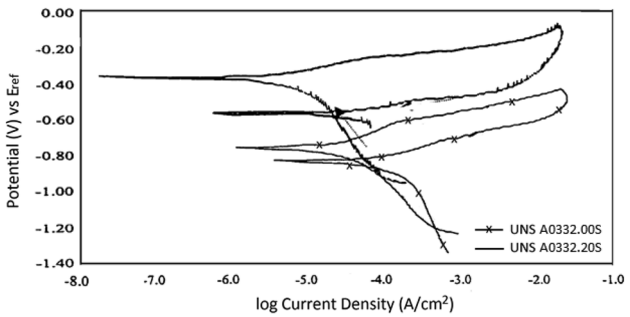

Fig. 3 Comparison of cyclic polarization curves for UNS A0332.00S and UNS A0332.20S

circuit/corrosion potential (E_{corr}) computed for each alloy sample shows that the greater the difference between these two values, the higher the pitting resistance of the respective alloy. This difference, $E_{corr} - E_{pit}$, is particularly used to determine the service performance of aluminum alloys in NaCl environments. UNS A0359.00S alloy has the greatest value of $E_{corr} - E_{pit}$ among the four alloys used (0.1550V). UNS A0332.00S, UNS A0359.20S, and UNS A0332.20S have respective $E_{corr} - E_{pit}$ values of 0.1527, 0.1386, and 0.1236 V. UNS A0359.00S alloy displayed superior pitting resistance in NaCl solution compared to the other alloy samples. As earlier mentioned, the presence of chloride ions in aqueous media in contact with aluminum metal or aluminum alloys causes pitting attack. The cathodic reaction mechanism taking place during pitting corrosion of aluminum alloys in NaCl solution reduces oxygen to hydroxyl ion. The analogous anodic reaction takes place according to the following equations [58]:

$$Al + 3H_2O \rightarrow Al(OH)_3 + 3H^+ + 3e^- \quad \text{(Eq 6)}$$

$$Al + 2H_2O \rightarrow AlO(OH) + 3H^+ + 3e^- \quad \text{(Eq 7)}$$

$$Al + 3/2H_2O \rightarrow Al_2O_3 + 3H^+ + 3e^- \quad \text{(Eq 8)}$$

The presence of oxygen in the proximity of the intermetallic compound has a strong influence on the reduction reaction process; however, in the presence of chloride ion, the reactions are of the form [59]:

$$Al(OH)^{+2} + Cl^- \rightarrow Al(OH)Cl^+ \quad \text{(Eq 9)}$$

$$Al(OH)Cl^+ + H_2O \rightarrow Al(OH)2Cl + H^+ \quad \text{(Eq 10)}$$

The reactions above are responsible for the formation of corrosion products within the proximity of intermetallic particles. In the deaerated condition, the cathodic reaction is as follows (Eq 11):

$$H_2O + e^- \rightarrow OH^- + H_{(ad)} \quad \text{(Eq 11)}$$

Under this condition the hydroxide protective layer does not adhere strongly to the alloy surface, and thus is unable to prevent the dissolution of the alloy matrix and could not create suitable resistance for aluminum against corrosion. The Cl^- considerably enhances the initiation and propagation of the pits through an autocatalytic process. Positive metallic cations accumulate in the pits due to anodic

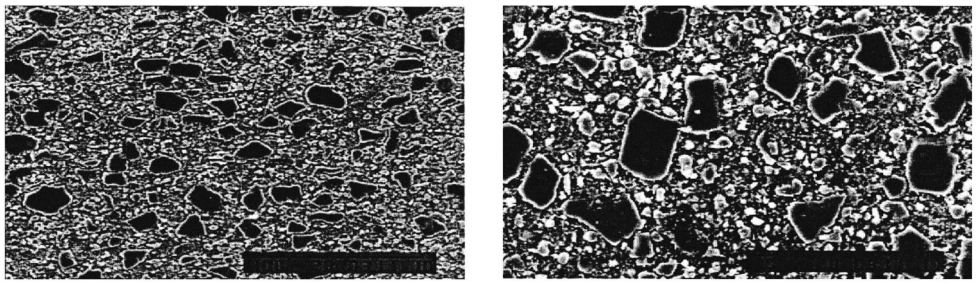

Fig. 4 Micrograph of non-corroded UNS A0332.20S sample

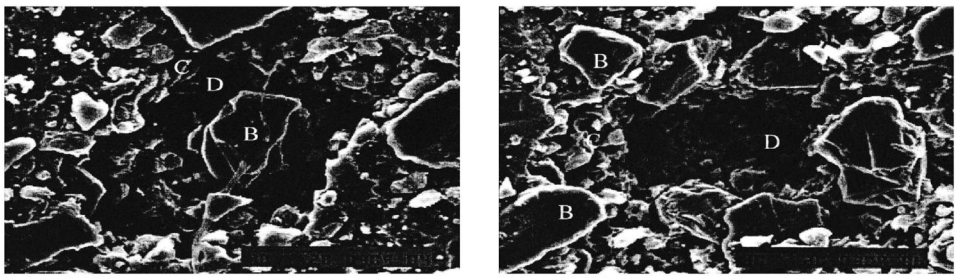

Fig. 5 Micrograph of corroded UNS A0332.20S sample

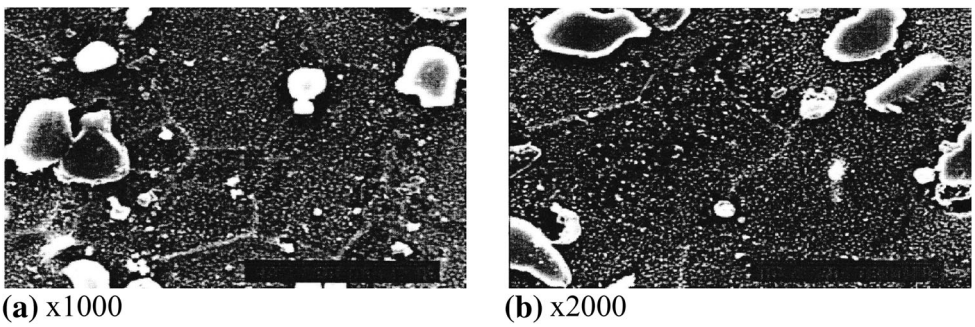

Fig. 6 Micrograph of non-corroded UNS A0332.00S sample

dissociation and metal degradation. The Cl^- ions also concentrate in the pits as a result of the metal cations and facilitate the reaction of the positive cations with H_2O to form OH^- corrosion product and H^+ ions. The pits being mildly acidic accelerate the corrosion process [60].

Micro-analytical Studies

Micrographs from scanning electron microscopy are presented in Figs. 4, 5, 6, 7, 8, 9, 10, and 11. Energy dispersive spectroscopy (EDS) was used to study the elemental compositions of the pit surroundings for the four aluminum alloy samples. Four major elements were detected by EDS in UNS A0332.20S aluminum alloy (Fig. 12). The elements consist of aluminum (52.62% composition), silicon (23.47% composition), nickel (10.10% composition), and copper (13.81% composition). According to Mondolfo [61] on information guiding the formation of phases in aluminum alloys, the elements identified are most likely Cu_4NiAl_7 and $CuAl_2$ intermetallic phases around the pit circumference. Based on this, the site will be anodic relative to the alloy matrix if these elements only are responsible for the redox mechanism responsible for alloy degradation. In another perspective, the areas containing the suspected intermetallic phases might be cathodic relative to the entire matrix.

The presence of copper in aluminum alloy is deliberately to improve its corrosion resistance properties, as a result of which the formation of phases between copper and other alloying elements are expected to provide adequate protection against corrosion in NaCl media. Hence, the other alloying elements or possibly the aluminum matrix might deteriorate selectively in the NaCl media, thus the suspected phases are left intact within the pit region. Three major elements were detected in UNS A0332.00S alloy, from EDS results in Fig. 13. The elements are aluminum (76.63% composition), silicon (11.18% composition), and copper (12.19% composition). There is the possibility of

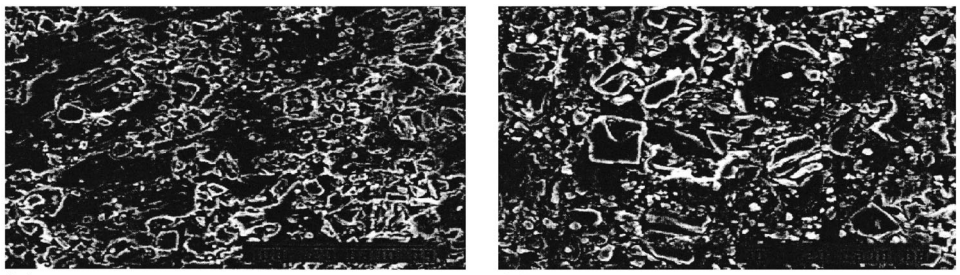

Fig. 7 Micrograph of corroded UNS A0332.00S sample after weight loss

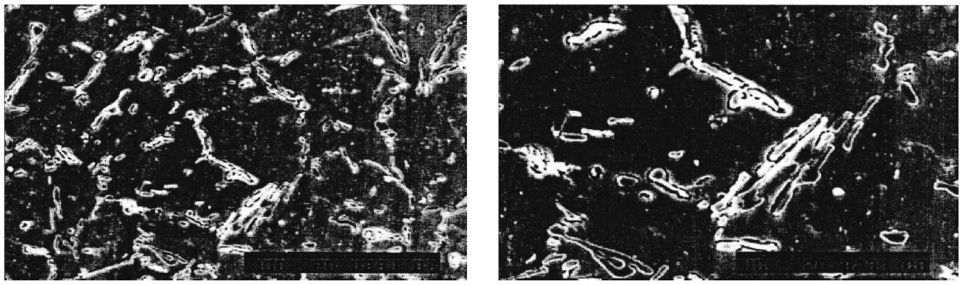

Fig. 8 Micrograph of non-corroded UNS A0359.00S sample

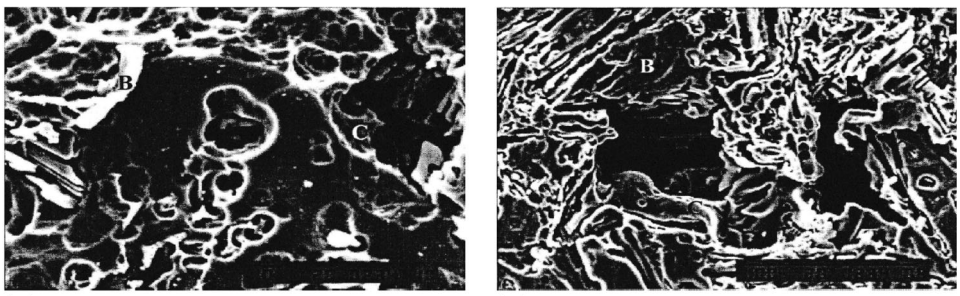

Fig. 9 Micrograph of corroded UNS A0359.00S sample after weight loss

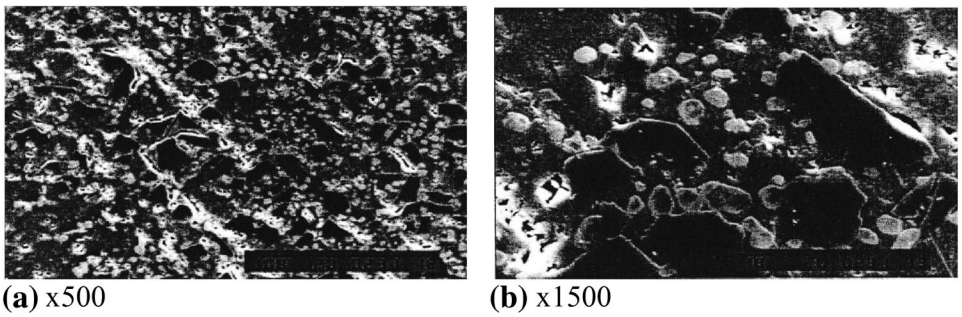

Fig. 10 Micrograph of non-corroded UNS A0359.20S sample

$CuAl_2$ intermetallic phase formation in the pit domain as earlier mentioned in the reinforced counterpart (UNS A0332.20S alloy). This is due to the formation of a single type of intermetallic phase within the pit's vicinity.

EDS results for the UNS A0359.00S alloy (Fig. 14) depicts four major elements within the pit's vicinity. The elements consist of aluminum (90.47% composition), silicon (3.06% composition), copper (1.48% composition), and magnesium (4.99% composition). Three possible major intermetallic phases can be recognized i.e., $Cu_2Mg_8Si_6Al_5$, Mg_2Si, and $CuMg_4Al_6$ [61]. The possible roles of these phases are explained in a similar manner as earlier illustrated. Figure 15 shows the EDS analysis of surface structure of UNS A0359.20S alloy. The results

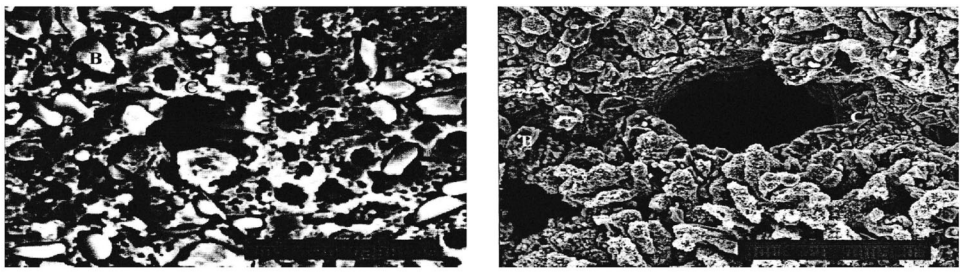

(a) x500 **(b)** x1000

Fig. 11 Micrograph of corroded UNS A0359.20S sample

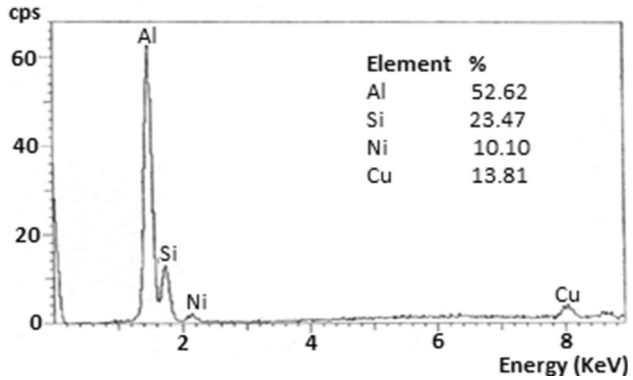

Fig. 12 EDS analysis of UNS A0332.20S showing elemental constituents in pit's surrounding

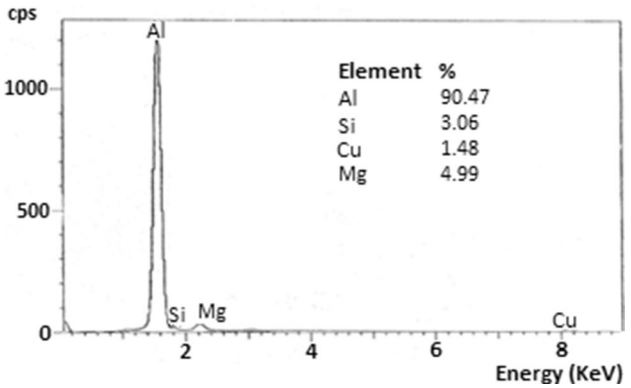

Fig. 14 EDS analysis of UNS A0359.00S showing elemental constituents in pit's surrounding

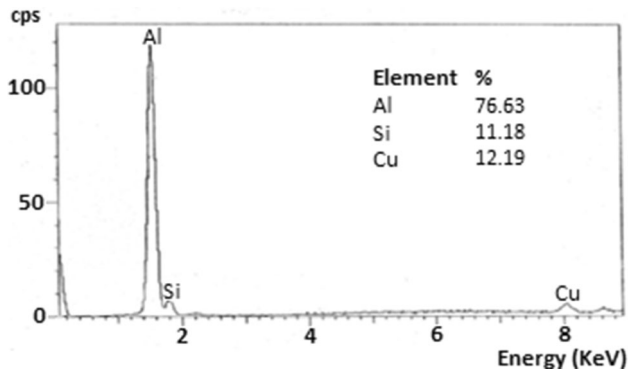

Fig. 13 EDS analysis of UNS A0332.00S showing elemental constituents in pit's surrounding

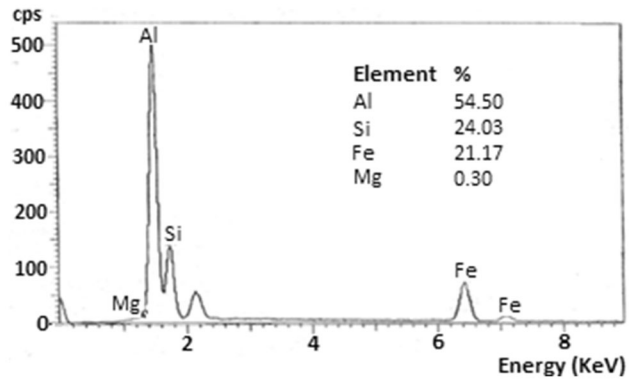

Fig. 15 EDS analysis of UNS A0359.20S showing elemental constituents in pit's surrounding

indicate the presence of four major elements in the pit's surrounding consisting of aluminum (54.50% composition), silicon (24.03% composition), iron (21.17% composition), and magnesium with (0.30% composition). Fe_2SiAl_5 and Mg_2Si intermetallic phases were possibly formed in the pit region based on the results.

The composition of the reinforcing particles are shown with EDS analysis (Fig. 16), consisting of aluminum (19.03% composition), silicon (70.34% composition), and carbon (10.63 % composition). A predominant agglomeration of SiC particles were formed in the area of alloy degradation. This supports the findings of Trazaskoma

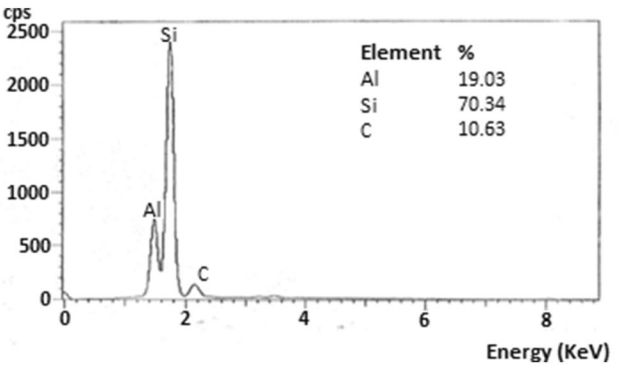

Fig. 16 EDS analysis of reinforced particles

[62]. In addition to the observations, it was found that the number of pits formed on the reinforced alloys is significantly higher than the unreinforced alloys. Aggregate calculation was achieved through observation of 0.6 cm^2 corroded areas, microscopically for each of the alloys. This investigation confirms that improved corrosion resistance exhibited by the unreinforced alloys is due to the presence of lower number of pits compared to the reinforced alloys.

Conclusion

Investigation of the effect of intermetallic phases on the corrosion of aluminum silicon carbide (Al-SiC_p) composites concludes that aluminum alloys reinforced with SiC are more susceptible to corrosion attack in NaCl environments than the reinforced alloys. Comparison of the corrosion rate of UNS A0359.20S, UNS A0359.00S, UNS A0332.00S, and UNS A0332.20S alloys from potentiodynamic polarization tests and weight loss analysis showed that UNS A0359.00S and UNS A0332.00S both have a higher corrosion resistance coupled with a lower number of pits formed on the surface than UNS A0359.20S and UNS A0332.20S whose corrosion pits appear deeper. Cyclic polarization results showed that UNS A0359.00S has the highest differential value between E_{corr} (corrosion potential) and E_p (pitting potential). This is followed sequentially by values obtained for UNS A0332.00S, UNS A0332.20S, and UNS A0359.20S alloys. Intermetallic phases observed in the aluminum alloys appear to represent the weakened sites on the alloys where localized corrosion occurs. The result further confirms that intermetallic phases may significantly influence the corrosion behavior of the reinforced alloys compared to the unreinforced counterparts. Silicon-dominating particles were observed to be present at the mouth of the pits especially those alloys that are reinforced with SiC particles. This may have contributed significantly to the weakening of pit regions.

Acknowledgment The authors express their sincere appreciation to Mechanical Engineering Department, College of Engineering Sciences and Applied Engineering, King Fahd University of Petroleum & Minerals, Dhahran, 31261, KSA for the availability of equipment and services for the research.

References

1. D.M. Aylor, *Metals Handbook*, 9th edn. (ASM, Metal Park, OH, 1984), pp. 859–863
2. S.V. Nair, J.K. Tien, R.C. Bates, SiC-reinforced aluminum metal matrix composites. Int. Met. Rev. **30**(6), 275–290 (1985)
3. D.M. Aylor, R.M. Kain, Assessing the corrosion resistance of metal matrix composite materials in marine environments, in: *Recent Advances in Composites in the United States and Japan, ASTM STP 864*, ed. by J.R. Vinson, M. Taya (ASTM, Philadelphia, PA, 1983), pp. 632–647.
4. D.M. Aylor, P.J. Moran, Effect of reinforcement on the pitting behaviour of aluminum-based metal matrix composites. J. Electrochem. Soc. **132**, 1277–1284 (1985)
5. M.C. Portal, E.G. Wolff, Advances in structural composites, Paper No. AC14, presented to Society of Aerospace Materials Process Engineering, 12th National Symposium, Exhibit, Western Period, North Hollywood, CA, 1967
6. N. Deo, T.K.G. Namboodhir, Some corrosion characteristics of aluminum-mica particulate composites. Corros. Sci. **29**(10), 1215–1229 (1989)
7. E. McCafferty, G.K. Hubler, P.M. Natishan, Naval research laboratory surface modification program: ion beam and laser processing of metal surfaces for improved corrosion resistance. Mater. Sci. Eng. **86**, 1–17 (1987)
8. P.P.M. Natishan, E. McCafferty, G.K. Hubler, The effect of pH of zero charge on the pitting potential. J. Electrochem. Soc. **133**, 1061–1062 (1986)
9. W.L. Xu, T.M. Yue, H.C. Man, C.P. Chan, Laser surface melting of aluminum alloy 6013 for improving pitting corrosion fatigue resistance. Surf. Coat. Technol. **16–17**, 5077–5086 (2000)
10. R.M. Latanision, Corrosion resistance of rapidly quenched alloys, in: *Critical Issues in Reducing the Corrosion of Steels*, ed. by H. Leidheiser, S. Haruyama (NACE, Houston, TX, 1986), p. 182
11. A.H. Al-saffar, V. Ashworth, A.K.O. Balimov, D.J. Chivers, W.A. Grant, R.P.M. Procter, The effect of molybdenum ion implantation on the general and pitting corrosion behaviour of pure aluminum and high strength aluminum alloy. Corros. Sci. **20**(1), 127–144 (1980)
12. A.J. Sedriks, J.A.S. Green, D.L. Novak, Corrosion behavior of aluminum-boron composites in aqueous chloride solutions. Met. Trans. **2**(3), 871–875 (1971)
13. M.S.H. Bhat, M.K. Surappa, Corrosion behaviour of silicon carbide particle reinforced 6061/Al alloy composites. J. Mater. Sci. **26**(18), 4991–4996 (1991)
14. P.P. Trzaskoma, Pit morphology of aluminum alloy and silicon carbide/aluminum alloymetal matrix composites. Corrosion **46**(5), 402–409 (1990)
15. J. Wu, W. Liu, P. Li, R. Wu, Effect of matrix alloying elements on the corrosion resistance of C/Al composite materials. J. Mater. Sci. Lett. **12**(19), 1500–1501 (1993)
16. H. Sun, E.Y. Koo, H.G. Wheat, Corrosion Behavior of SiCp/6061 Al metal matrix composites. Corrosion **47**(10), 741–753 (1991)
17. R.C. Paciej, V.S. Agarwala, Influence of processing variables on the susceptibility of metal-matrix composites. Corrosion **44**, 680–684 (1988)
18. F.U. Yuechun, S.H.I. Nanlin, Z. Dezhi, Y. Rui, Microstructural changes of Ti-6Al-4V Matrix by the incorporation of continuous SIC fibers. J. Mater. Sci. Technol. **22**(4), 452–454 (2006)
19. P.P. Trzaskoma, Proceedings on the Effects of Silicon Carbide Whiskers on the Initiation and Propagation of Pits on Silicon Carbide/Aluminum Metal Matrix Composites, in: *10th Congress on Metallic Corrosion, Madras, India*, 1987.
20. P.P. Trzaskoma, E. McCafferty, C.R. Crane, Corrosion behaviour of SiC/Al metal matrix composites. J. Electrochem. Soc. **130**, 1804–1809 (1983)
21. P.P. Trzaskoma, Localized corrosion of metal matrix composites, in: *Environmental Effects in Advanced Materials*, ed. by H.J. Russell, E.R. Richard (The Minerals, Metals & Materials Society, Warrendale, PA, 1981), p. 249.
22. M.A. Streicher, Pitting corrosion of 18Cr-8Ni stainless steel. J. Electrochem. Soc. **103**(7), 375–390 (1956)
23. B.E. Wilde, J.S. Armijo, Influence of sulfur on the corrosion resistance of austenitic stainless steel. Corrosion **23**(7), 208–214 (1967)

24. Z. Szklarska-smialowska, Pitting corrosion of aluminum. Corros. Sci. **41**, 1743–1767 (1991)
25. J.R. Galvele, S.M. Demicheli, Mechanism of intergranular corrosion of Al-Cu alloys. Corros. Sci. **10**(11), 795–807 (1970)
26. I.L. Muller, J.R. Galvele, Pitting potential of high purity binary aluminum alloys—I. Al.Cu alloys. Pitting and intergranular corrosion. Corros. Sci. **17**, 179–189 (1977)
27. B. Mazurkiewicz, A. Piotrowski, The electrochemical behaviour of the Al2Cu intermetallic compound. Corros. Sci. **23**, 697–707 (1983)
28. Corrosion of Aluminum and Aluminum Alloys, http://www.totalmateria.com/Article14.htm. Accessed: 11 Feb 2016
29. H. Ezuber, A. El-houd, F. El-shawesh, A study on the corrosion behavior of aluminum alloys in seawater. Mater. Design **29**(4), 801–805 (2008)
30. E. Deltombe, M. Pourbaix, The electrochemical behavior of aluminum—potential pH diagram of the system AI-H_2O at 25°C. Corrosion **14**(11), 16–20 (1958)
31. B. Zaid, D. Saidi, A. Benzaid, S. Hadji, Effects of pH and chloride concentration on pitting corrosion of AA6061 aluminum alloy. Corros. Sci. **50**, 1841–1847 (2008)
32. H.M. Zakaria, Microstructural and corrosion behavior of Al/SiC metal matrix composites. Ain Shams Eng. J. **5**(3), 831–838 (2014)
33. F. Gnecco, A.M. Beccaria, Corrosion behaviour of Al–Si/SiC composite in sea water. Br. Corros. J. **34**(1), 57–62 (1999)
34. A. Pardo, M.C. Merino, S. Merino, M.D. López, F.M. Viejo, Carboneras. Influence of SiCp content and matrix composition on corrosion resistance in cast aluminum matrix composites in salt fog. Corros. Eng. Sci. Technol. **39**(1), 82–88 (2004)
35. B.J. Shamsul, B.Y. Zamri, R.A. Khairel, Comparative study of corrosion behavior of AA2014/15 Vol% Al_2O_3p and AA2009/20 Vol% SiCw. Portug. Electrochim. Acta. **26**(3), 291–301 (2008)
36. P.M. Natishana, W.E. O'Grady, Chloride ion interactions with oxide-covered aluminum leading to pitting corrosion: a review. J. Electrochem. Soc. **161**(9), C421–C432 (2014)
37. P. Schmuki, From Bacon to barriers: a review on the passivity of metals and alloys. J. Solid State Electrochem. **6**(3), 145–164 (2002)
38. G.S. Frankel, N. Sridhar, Review: understanding localized corrosion. Mater. Today **11**(10), 38–44 (2008)
39. I. Bennour, V. Maurice, P. Marcus, X-ray photoelectron spectroscopy study of the interaction of ultra-thin alumina films on NiAl alloys with NaCl solutions. Surf. Interface Anal. **42**(6-7), 581–587 (2010)
40. P. Marcus, V. Maurice, H.H. Strehblow, Localized corrosion (pitting): a model of passivity breakdownincluding the role of the oxide layer nanostructure. Corros. Sci. **50**, 2698–2704 (2008)
41. C.Y. Chao, L.F. Lin, D.D. MacDonald, A point defect model for anodic passive films I. Film growth kinetics. J. Electrochem. Soc. **128**, 1187–1194 (1981)
42. L.F. Lin, C.F. Chao, D.D. MacDonald, A point defect model for anodic passive films II. Chemical breakdown and pit initiation. J. Electrochem. Soc. **128**, 1194–1198 (1981)
43. M. Urquidi, D.D. MacDonald, Solute vacancy interaction model and the effect of minor alloying elements on the initiation of pitting corrosion. J. Electrochem. Soc. **132**, 555–558 (1985)
44. N.L. Sukiman, X. Zhou, N. Birbilis, A.E. Hughes, J.M.C. Mol, S.J. Garcia, X. Zhou, G.E. Thompson, Durability and corrosion of aluminum and its alloys: overview, property space, techniques and developments, in: *Aluminum Alloys—New Trends in Fabrication and Applications* ed. by Z. Ahmad (InTech, Rijeka, 2012).
45. S.M. Hirth, G.J. Marshall, S.A. Court, D.J. Lloyd, Effects of Si on the aging behaviour and formability of aluminum alloys based on AA6016. Mater. Sci. Eng. A. **319–321**, 452–456 (2001)
46. M. Usta, M.M.E. Glicksman, R.N. Wright, The effect of heat treatment on Mg_2Si coarsening in aluminum 6105 alloy. Met. Mater. Trans. A. **35A**(2), 435–438 (2004)
47. O. Stelling, A. Irretier, O. Kessler, P. Krug, B. Commandeur, New light-weight aluminum alloys with high Mg_2Si-content by spray forming. Mater. Sci. Forum. **519–521**, 1245–1250 (2006)
48. F. Eckermann, F.T. Suter, P.J. Uggowitzer, A. Afseth, P. Schmutza, The influence of MgSi particle reactivity and dissolution processes on corrosion in Al–Mg–Si alloys. Electrochim. Acta. **54**(2), 844–855 (2008)
49. F.I. Zeng, Z.I. Wei, J.F. Li, C.X. Li, X. Tan, Z. Zhang, Z.Q. Zheng, Corrosion mechanism associated with Mg_2Si and Si particles in Al–Mg–Si alloys. Trans. Nonferrous Met. Soc. China. **21**(12), 2559–2567 (2011)
50. V. Guillaumin, G. Mankowski, Localized corrosion of 2024 T351 aluminum alloy in chloride media. Corros. Sci. **41**(3), 421–438 (1998)
51. M.H. Larsen, J.C. Walmsley, O. Lunder, R.H. Mathiesen, K. Nisancioglu, Intergranular corrosion of copper-containing AA6xxx AlMgSi aluminum alloys. J. Electrochem. Soc. **155**(11), C550–C556 (2008)
52. I.L. Muller, J.R. Galvele, Pitting potential of high purity binary aluminum alloys—II. AlMg and AlZn alloys. Corros. Sci. **17**(12), 995–1007 (1977)
53. B. Mazurkiewicz, A. Piotrowski, The electrochemical behaviour of the Al_2Cu intermetallic compound. Corros. Sci. **23**(7), 697–707 (1983)
54. J.R. Scully, T.O. Knight, R.G. Buchheit, D.E. Peebles, Electrochemical characteristics of the Al_2Cu, Al_3Ta and Al_3Zr intermetallic phases and their relevancy to the localized corrosion of Al alloys. Corros. Sci. **35**(1–4), 185–195 (1993)
55. R.G. Buchheit, Electrochemistry of θ(Al_2Cu), S(Al_2CuMg) and T1(Al_2Cu–Li) and localized corrosion and environment assisted cracking in high strength Al alloys. Mater. Sci. Forum. 331(II), (2000).
56. N. Birbilis, M.K. Cavanaugh, R.G. Buchheit, Electrochemical behavior and localized corrosion associated with Al_7Cu_2Fe particles in aluminum alloy 7075-T651. Corros. Sci. **48**(12), 4202–4215 (2006)
57. E. Andres, O. Juan, R. Edmundo, H. Francisco, A. Daniela, G. Juanluis, Oxygen reduction on Cu_1, $Mn_{16}O_4$ spinel particles composite electrodes effect of particles size. J. Chilean Chem. Soc. (2014). doi:10.4067/S0717-97072014000200023
58. R. Gundersen, K. Nisancioglu, Cathodic protection of aluminum in seawater. Corrosion **46**(4), 279–285 (1990)
59. S.Y. Luo, Y.C. Zheng, M.C. Li, Effect of Cavitation on corrosion behavior of 20SiMn low-alloy steel in 3% sodium chloride solution. Corrosion. **59**(7), 597–605 (2003)
60. R.T. Loto, Pitting corrosion evaluation of austenitic stainless steel type 304 in acid chloride media. J. Mater. Environ. Sci. **4**(4), 448–459 (2013)
61. L.F. Mondolfo, *Aluminum Alloys: Structure and Properties* (Butterwort, London, 1976), pp. 534–774
62. P.P. Trzaskoma, Pit morphology of aluminum alloy and silicon carbide/aluminum alloy metal matrix composites. Corrosion **46**(5), 402–409 (1990)